Magmatic-hydrothermal molybdenum isotope fractionation and its relevance to the igneous crustal signature

Nicolas D. Greber[1,*], Thomas Pettke[1] and Thomas F. Nägler[1]

[1] Institute of Geological Sciences, University of Bern, Baltzerstrasse 3, 3012 Bern, Switzerland

*Corresponding author. E-mail: greber@geo.unibe.ch

Addresses:

Nicolas D. Greber:

Institute of Geological Sciences, University of Bern, Baltzerstrasse 3, CH-3012 Bern; Tel: +41 31 631 8533;

E-mail: greber@geo.unibe.ch

Thomas Pettke:

Institute of Geological Sciences, University of Bern, Baltzerstrasse 3, CH-3012 Bern; Tel: +41 31 631 5059;

E-mail: pettke@geo.unibe.ch

Thomas F. Nägler:

Institute of Geological Sciences, University of Bern, Baltzerstrasse 3, CH-3012 Bern; Tel: +41 31 631 8752;

E-mail: naegler@geo.unibe.ch

Abstract

We analyzed the Mo isotope composition of a comprehensive series of molybdenite samples from the porphyry-type Questa deposit (NM, USA), as well as one rhyolite and one granite sample, directly associated with the Mo mineralization. The δ^{98}Mo of the molybdenites ranges between -0.48‰ and +0.40‰, with a median at -0.05‰. The median Mo isotope composition increases from early magmatic (-0.29‰) to hydrothermal (-0.05‰) breccia mineralization (median bulk breccia = -0.17‰) to late stockwork veining (+0.22‰). Moreover, variations of up to 0.34‰ are found between different molybdenite crystals within an individual hand specimen. The rhyolite sample with 0.12 μg g^{-1} Mo has δ^{98}Mo = -0.57‰ and is lighter than all molybdenites from the Questa deposit, interpreted to represent the igneous leftover after aqueous ore fluid exsolution. We recognize three Mo isotope fractionation processes that occur between ca. 700 and 350°C, affecting the Mo isotope composition of magmatic-hydrothermal molybdenites. Δ_1Mo: Minerals preferentially incorporate light Mo isotopes during progressive fractional crystallization in subvolcanic magma reservoirs, leaving behind a melt enriched in heavy Mo isotopes. Δ_2Mo: Magmatic-hydrothermal fluids preferentially incorporate heavy Mo isotopes upon fluid exsolution. Δ_3Mo: Light Mo isotopes get preferentially incorporated in molybdenite during crystallization from an aqueous fluid, leaving behind a hydrothermal fluid that gets heavier with progressive molybdenite crystallization. The sum of all three fractionation processes produces molybdenites that record heavier δ^{98}Mo compositions than their source magmas. This implies that the mean δ^{98}Mo of molybdenites published so far (~0.4‰) likely represents a maximum value for the Mo isotope composition of Phanerozoic igneous upper crust.

Keywords: molybdenum; isotope; fractionation; molybdenite; hydrothermal

1. Introduction

Molybdenum isotope ratios are mainly employed to model paleo-redox conditions of ancient Earth's hydrosphere (e.g., Arnold et al., 2004; Wille et al., 2007). One critical parameter to this type of modelling is the isotopic composition of the continent derived Mo input to the oceans. Its value was approximated either by analysis of silicate rocks (Siebert et al. 2003), river water (Archer and Vance 2008) or molybdenites (e.g., Barling et al., 2001). Audétat et al. (2011) indentified molybdenite as an accessory magmatic phase in 13 out of 27 felsic magmatic systems, showing that this mineral is more abundant and potentially more important in the global Mo cycle than previously suspected. However, an added complexity emerges from the wide range of δ^{98}Mo values observed in molybdenites from various ore deposits (Hannah et al., 2007; Malinovsky et al., 2007; Mathur et al., 2010; Pietruszka et al., 2006; Wieser and DeLaeter, 2003). Moreover, a range in δ^{98}Mo of 1.35‰ - much larger than that of all published Mo isotope compositions for igneous rocks to date - has been reported for a single molybdenite occurrence, suspected to be the product of magmatic source variability and fractionation upon molybdenite precipitation from a hydrothermal fluid (Greber et al., 2011). Nevertheless, molybdenites are still under discussion and in use to define the Mo isotope crustal input signature to the ocean (e.g. Czaja et al., 2012; Dahl et al., 2011). However, the direction of, and the reason for, Mo isotope fractionation in magmatic and hydrothermal processes have remained unknown to date. This makes the interpretation of the δ^{98}Mo values of molybdenites for the continental runoff difficult. First speculations looking at the δ^{98}Mo values of various deposits suggested that Rayleigh distillation during molybdenite precipitation was responsible for isotope fractionation (Hannah et al., 2007; Mathur et al., 2010). However, the data in Greber et al., (2011) cannot be explained by a single Mo isotope fractionation process. Therefore, in an attempt to better understand both the significance of molybdenite δ^{98}Mo for estimating the Mo isotope signature of igneous crust available to erosion and the Mo isotope fractionation processes in magmatic-

64 hydrothermal environments, we investigated the Mo isotope composition of molybdenite crystallized from
65 late magmatic to hydrothermal fluids. The genesis of the Questa porphyry Mo deposit is exceptionally
66 well characterised, both in terms of geochemistry and petrology (e.g., Cline and Bodnar, 1994; Klemm et
67 al., 2008; Ross et al., 2002). Therefore, it is an ideal candidate to improve our knowledge about Mo
68 isotope fractionation processes at the magmatic-hydrothermal transition and during hydrothermal
69 molybdenite crystallization, conditions for which reliable information is scarce.
70 Three different Mo fractionation processes are identified here, occurring at temperatures of
71 between ca. 700 and 350 °C, which account for δ^{98}Mo variability in the molybdenite exceeding 0.8‰.
72 These data add to the growing body of evidence for prominent high-temperature isotope fractionation of
73 Mo, with profound implications for the global Mo isotope cycle.
74

75 ## 2. Geology

76 The Questa porphyry-Mo-only deposit, one of the largest of its kind, is hosted by the late
77 Oligocene Questa Caldera within the Latir volcanic field in the Rocky Mountains of New Mexico, USA
78 (e.g., Cline and Bodnar, 1994; Johnson et al., 1990; Lipman, 1988; see Figure 1). The mineralization and
79 associated felsic magmatism occurred at the beginning of extensive tectonic movements along the Rio
80 Grande Rift, marking the incipient breakup of the early Proterozoic crust formed during the assembly of
81 Laurentia (e.g., Karlstrom et al., 2005). The Questa porphyry Mo deposit consists of distinct ore bodies,
82 which are located around or to the west of the Sulfur Gulch pluton (Klemm et al. 2008, see Figure1).
83 Czamanske et al., (1990) dated the molybdenite mineralization to 24.2 to 24.1 Ma using Ar-Ar. Newer
84 Re-Os data of molybdenites tend to be older at 24.76 to 24.51 Ma (Rosera et al., 2013). The granitic
85 Sulfur Gulch, Red River and Bear Canyon plutons show a younging from east to west, where the Red

River is the oldest with an age of about 24.94 Ma and the Bear Canyon the youngest granitic pluton with an age between 24.54 to 24.37 Ma (Zimmerer and McIntosh 2012).

Detailed geologic, fluid inclusion and geochemical investigations (Klemm et al., 2008; Cline and Bodnar, 1994; Ross et al., 2002) demonstrate that the Questa Mo mineralization formed in two distinct hydrothermal stages documented by the magmatic-hydrothermal breccia (MHBX) and the stockwork veins (STW; see Figure 2). The MHBX was formed at temperatures above 350 °C and the STW between 300 and 410°C (Klemm et al., 2008). The MHBX itself grades from an igneous facies proximal to the source(s) towards a hydrothermal facies, while the STW represents a single stage formation cutting the MHBX (Klemm et al., 2008). The Questa Caldera is underlain by a batholith at shallow depth connecting the mineralized and associated barren subvolcanic intrusions (Lipman, 1988). This suggests that magmatic-hydrothermal ore formation is linked to a large magmatic reservoir. Increasing Cs contents of fluid inclusions from the MHBX to the STW samples document that fluid exsolution from an increasingly fractionated magma occurred in two distinct pulses; hence, the Questa Mo mineralization records a protracted magmatic-hydrothermal history with molybdenite mineralization at temperatures between 410-350°C (Klemm et al., 2008). According to recent Re-Os molybdenite ages (Rosera et al., 2013), MHBX and STW are contemporaneous to within 0.1 Ma; hence, the two discrete mineralization stages as identified by Klemm et al. (2008) by cross-cutting relationships and variably evolved magmatic-hydrothermal fluid compositions are sourced in magma batches recording different degrees of fractional crystallization at ore fluid exsolution. This strongly indicates the presence of a zoned magma reservoir at depth. Sampling of such discrete evolutionary source zones by texturally distinct mineralization stages thus greatly aids in constraining the direction and extent of igneous (magmatic-hydrothermal) Mo isotope fractionation. Cline and Bodnar (1994) and Klemm et al. (2008) report

undisturbed microthermometric fluid inclusion systematics, showing that the Questa deposit has not been overprinted by metamorphism.

3. Sample material and analytical techniques

Molybdenite samples, covering the entire mineralization from the MHBX to the STW in the so-called D ore body in the southwest zone of the Questa deposit (see Ross et al., 2002 and Figure 1), were characterized for their Mo isotope composition. Eleven samples are from the thoroughly characterised sample material used in Klemm et al. (2008), while one sample from an old collection (Nr.4, see Table 1) is of unknown mineralization stage. From each hand specimen, several individual molybdenite analyses using different crystals were performed (see Table 1). Magmatic rocks associated with the Mo mineralization are almost always altered hydrothermally. We measured the Mo isotope composition of a porphyry rhyolite dike that intruded contemporaneously with the molybdenite mineralization (McKinlay, 1988) and of a sample from the ca. 1 Ma younger Bear Canyon granite. We chose these two samples because thin section microscopy identified only moderately altered amphibole and plagioclase. The Bear Canyon granite is directly associated with a molybdenite mineralization named Log Cabin Deposit, which is situated about 5 km to the west of the Questa D ore body.

Sample processing for Mo concentration and isotope ratio analysis followed procedures reported in Greber et al., (2011). The δ^{98}Mo compositions were analysed using a double focusing Nu Instruments^{TM} MC-ICP-MS system. The use of a double-spike allowed for simultaneous determination of the Mo isotope composition and the Mo concentration. Measurement routine and double spike calibration are described in detail in Siebert et al., (2001) and Greber et al. (2012). The Mo isotope composition is conventionally given as delta notation based on the 98/95Mo ratio. The Mo isotope data standardization is done following the suggestion of Nägler et al., (2013), i.e. δ^{98}Mo composition of NIST SRM 3134 is set to +0.25‰. The

resulting values are directly comparable to all our previously published data. Analytical precision is better than ±0.10‰ (2SD) for both, liquid and solid standard reference materials processed through extraction chemistry (NIST SRM 3134 solution; SRM 610 and 612 glasses from NIST; see Greber et al., 2012). The error of a measurement is therefore ≤0.10‰ (2SD) and all Mo isotope composition data from here on are subject to this uncertainty, unless stated otherwise.

Major and selected trace element concentrations of the two igneous bulk rock samples (see Table S.1) were determined by XRF and LA-ICP-MS on $Li_2B_4O_7$ glasses. XRF measurements were performed on an Axios, PANalytical wavelength-dispersive X-ray fluorescence spectrometer at the Institute of Geochemistry and Petrology, Department of Earth Sciences ETH, Zurich, Switzerland. LA-ICP-MS was done using an ELAN DRCe quadrupole mass spectrometer (QMS; Perkin Elmer, Canada) couplet with a pulsed 193 nm ArF Excimer laser (Lambda Physik, Germany) and an energy-homogenized (Microlas, Germany) beam profile. Details on the setup and optimization strategies can be found in Pettke (2008).

4. Results

We made 42 individual analyses using different molybdenite crystals from the 12 different hand specimens to investigate inter- and intra-sample δ^{98}Mo variations. In addition, two individual analyses of the rocks associated with the Questa Caldera were measured for their Mo concentration and isotope composition. The δ^{98}Mo values of molybdenites range from -0.48‰ to +0.40‰, while the rhyolite and Bear Canyon granite averages are -0.57‰ and -0.15‰, respectively (Figure 3; Table 1). The δ^{98}Mo median of all molybdenites is -0.05‰. Each mineralization stage covers a range in δ^{98}Mo (Figure 3) that is statistically discrete based on null hypothesis calculations using the one-tailed students *t*-test (t-value at 95 % confidence). A conspicuous trend from light to heavier values from the igneous (median = -0.29‰) to the hydrothermal MHBX (median = -0.05‰), to the STW (median = +0.22‰) exists. All measured

154 molybdenites have a heavier Mo isotope composition than the rhyolite. Note that this rhyolite with a bulk
155 rock Mo concentration of 0.12 µg g^{-1} and its δ^{98}Mo value of -0.57‰ represents the lightest Mo isotope
156 composition reported for igneous rocks so far. The Bear Canyon granite sample possesses ca. 40 µg g^{-1}
157 Mo (MC-ICP-MS and LA-ICP-MS show identical values) with a Mo isotope composition at about the
158 centre of the MHBX molybdenites (-0.17‰; Figure 3). The XRF bulk rock data (see Table S.1) reveal that
159 the concentrations of the major elements of both igneous rocks closely resemble each other (see Figure
160 S.1). The SiO_2 content is above 76 wt% and the total alkali around 8.5 wt%. Trace element concentrations,
161 except Mo for the Bear Canyon sample, are generally low (e.g. Zn, Cu, Ni, Cr, V, Th and U). Finally,
162 molybdenite sample Nr. 4 of unknown mineralization type possesses a δ^{98}Mo of ca. 0.35‰, suggesting
163 that it belongs to the STW stage.

164 Besides this overall trend in δ^{98}Mo, intra-sample variations also occur. This is documented by
165 individual analysis of different molybdenite crystals from within the same hand specimen, between which
166 the δ^{98}Mo values can range over 0.34‰ (e.g., QDU 2.2). These systematic inter- and intra-sample
167 variations are similar to, but less extreme than, those reported for a small molybdenite mineralization from
168 the Swiss Alps (Greber et al., 2011).

169

170 ## 5. Discussion

171 ### 5.1. Magmatic and hydrothermal molybdenum isotope fractionation

172 The δ^{98}Mo data presented here infer that the Mo isotope composition of the hydrothermal fluids
173 and their potential source magmas are variable. The following discussion thus attempts to identify the
174 processes that caused these δ^{98}Mo variations of molybdenites within and between successive
175 mineralization pulses and even in individual molybdenite hand specimens. The variation of the data set
176 could be reduced by eliminating outliers, e.g., sample QDS3.2 c, or by assuming that the sample QDS4.8

contained igneous MHBX molybdenite (Table 1). Resulting changes in average values and median for the successive mineralization stages are not significant, however; hence, no outlier rejection was made.

The different signatures of the three stages in the late magmatic to hydrothermal evolution of this igneous system are interpreted to document at least three different Mo isotopes fractionation mechanisms (Figure 2). A first Mo isotope fractionation process, named Δ_1Mo here, refers to increasing δ^{98}Mo in magma with progressive fractional crystallization. Molybdenum isotope fractionation also occurs at the magmatic-hydrothermal transition, i.e., upon Mo partitioning into aqueous fluid exsolved from crystallizing silicic magma, here referred to as Δ_2Mo. Finally, Mo isotope fractionation during hydrothermal molybdenite precipitation (Δ_3Mo) is indicated. These three processes are now addressed in detail.

1. *Δ_1Mo:* Klemm et al., (2008) have demonstrated that the discrete molybdenite mineralizing stages, MHBX and STW, formed from distinct stages of fluid exsolution from progressively more fractionated source magma. Since it is likely that aqueous fluid exsolution for the MHBX and later STW stages occurred at similar P-T conditions (Klemm et al., 2008), differences in the Mo isotope fractionation factor between the silicate melt and the aqueous fluid (Δ_2Mo; see below) are unlikely. Hence, the ~0.4‰ heavier average δ^{98}Mo in STW than in MHBX molybdenites (Figure 3 and Table 1) infers that heavy Mo isotopes get preferentially enriched in the residual melt of subvolcanic magma chambers with progressive magma crystallization. This finding is perfectly in line with recent data from the Kos island arc volcanic system (Voegelin et al., submitted).

2. *Δ_2Mo*: This second Mo isotope fractionation process is based on the assumption that the rhyolite dike sample tapped the same, large magma chamber that sourced the Mo mineralization. The low Mo

200 content, 0.12 μg g^{-1} (Table 1), is much below Mo concentrations expected for evolved silicic magmas
201 and suggests that the rhyolite represents residual magma after aqueous fluid exsolution. This genesis is
202 also suggested by low concentrations of Cu, Zn, Pb, relative to the high field strength elements (e.g.,
203 Th, Ta, Zr; compare Zajacz et al., 2008). Indeed, measured Mo partition coefficients between exsolved
204 aqueous fluid and residual silicate melt of the order of 10 (Audétat and Pettke, 2003; Audétat, 2010;
205 Zajacz et al., 2008) imply that the source magma had some 1.2 μg g^{-1} of Mo prior to fluid exsolution,
206 consistent with common rhyolithic bulk rock data published so far (Arnórsson and Óskarsson 2007;
207 Kuroda and Sandell 1954; Raimbault and Burnol 1998). The δ^{98}Mo signatures of the MHBX (δ^{98}Mo =
208 -0.17‰) and the STW (δ^{98}Mo = 0.22‰) are heavier than the δ^{98}Mo of the rhyolite dike sample
209 (δ^{98}Mo = -0.57‰), implying that isotope fractionation towards heavier Mo occurs when Mo partitions
210 from hydrous silicate melt into the exsolving hydrothermal fluid phase. After the first fluid exsolution,
211 a lighter melt is left behind. Therefore, two different magma batches with a different crystallization
212 degree (see Δ_1Mo) were responsible for the two mineralization stages, perfectly in line with the
213 magmatic-hydrothermal fluid compositional evolution determined by Klemm et al. (2008). The bulk
214 rock δ^{98}Mo of -0.16‰ of the Bear Canyon granite (Table 1) does not fit the scenario of representing
215 the igneous leftover. The Mo concentration of 40.5 μg g^{-1} exceeds bulk upper crust values (1.0 to 1.5
216 μg g^{-1}; GERM, January 2013) by more than an order of magnitude, but it corresponds well to the
217 highest Mo concentrations of most extremely fractionated melt inclusions reported so far (Audétat and
218 Pettke, 2003; Audétat et al., 2011). This implies that the Bear Canyon pluton either (1) did not exsolve
219 an aqueous fluid prior to crystallization (hence, all Mo stayed in the magma), or (2) that the Bear
220 Canyon pluton sample analyzed here was affected by magmatic-hydrothermal overprint highly
221 enriched in Mo. Given that Mo is highly incompatible in silicic magma and will thus get enriched with
222 progressive fractionation analogous to Cs, hypothesis (1) would require very high Cs contents in the

223 Bear Canyon sample (in analogy to melt inclusion data; Audetat and Pettke, 2003). However, the Cs
224 content at 1.3 μg g^{-1} is very low, suggesting (a) that this granite may also represent an igneous leftover
225 after fluid exsolution that then (b) got mineralized by Mo ore fluid, as is also consistent with elevated
226 Cu and Zn concentrations (see Figure S.1). The latter hypothesis is fully consistent with the fact that
227 the δ^{98}Mo of the Bear Canyon granite and the median of the MHBX molybdenites are identical
228 (Figure 3). We thus infer that the Mo concentration and the Mo isotope composition of the Bear
229 Canyon granite are predominantly characterized by the hydrothermal molybdenite mineralization
230 possibly associated with the Log Cabin Mo Deposit. Clearly, the δ^{98}Mo of the Bear Canyon granite
231 does not represent the signature of the igneous leftover magma after magmatic-hydrothermal fluid
232 exsolution.
233
234 3. $\Delta_3 Mo$: The prominent variability in δ^{98}Mo within individual molybdenite mineralizing stages (Figure
235 3) and even within individual hand specimens suggests that Mo isotope fractionation occurred during
236 (a) molybdenite precipitation from the hydrothermal fluid, possibly in addition to (b) Mo isotope
237 fractionation due to fluid phase separation into brine and vapour (Klemm et al., 2008). This
238 fractionation process is likely to be driven by redox-related isotope fractionation similar to light Mo
239 incorporation into crystallizing silicates during progressive fractional crystallization (Voegelin et al.,
240 submitted). The lighter δ^{98}Mo in the magmatic facies of the MHBX relative to that in the intimately
241 associated hydrothermal facies of the MHBX indicates that Mo incorporated into molybdenite is also
242 lighter than residual Mo in the hydrothermal fluid. This process potentially results in locally restricted
243 Rayleigh distillation as suggested by Hannah et al. (2007) and Mathur et al. (2010), which can
244 partially account for the within-sample δ^{98}Mo variability of molybdenites commonly observed.
245 Consequently, a δ^{98}Mo range of hydrothermal molybdenites is expected to result from progressive

molybdenite precipitation during fluid cooling in shallow, open hydrothermal systems. Yet another hydrothermal Mo isotope fractionation process may be phase separation of the hydrothermal fluid into coexisting brine and vapour and Mo partitioning between them ("fluid boiling") that is much more difficult to assess, however. According to experimental results on hydrated Mo-oxy complexes (Rempel et al., 2009), prominent fractions of Mo may be transported in a vapour phase. Natural assemblages of coexisting brine and vapour (Audétat and Pettke, 2003; Klemm et al., 2007), however, indicate preferential partitioning of Mo into the brine by an order of magnitude, consistent in trend with recent experimental data highlighting the importance of Mo complexation (Zhang et al., 2012). If *liquid - vapour* fractionation of Mo isotopes is of similar order as those documented here for *crystal - melt* and *aqueous fluid - melt* fractionations, precipitation of molybdenite from brine and vapour should further add to the Mo isotope variability of hydrothermal molybdenite from individual mineralization stages.

5.2. Potential chemical reactions resulting in high-T Mo isotope fractionation

It can only be speculated here about potential chemical reactions effecting Mo isotope fractionation at temperatures between ca. 700 and 350 °C. Most likely, these are related to changes in the oxidation state (Mo^{4+}, Mo^{5+}, and Mo^{6+}) and Mo speciation between silicate melt, aqueous fluid, crystals, and possibly also between saline brine and low-salinity vapour. While it is clear that Mo in molybdenite exists as Mo^{4+}, no definitive answer is possible for common rock-forming minerals. However, based on the charge and radius of Mo^{4+} and its main substitution for Ti^{4+}, Fe^{2+} and Fe^{3+} in ilmenite and magnetite (Kuroda and Sandell 1954), it is assumed to be also incorporated predominantly as Mo^{4+}. In the magmatic system described in Voegelin et al. (submitted), the hydrous minerals amphibole and biotite are main silicate carriers of Mo and they show preferred incorporation of light Mo isotopes. In contrast, Mo^{6+}

predominates in silicate melts at typical oxygen fugacities in igneous systems (Holzheid et al., 1994; O'Neill and Eggins, 2002).

Molybdenun isotopic fractionation in response to a reduction of the oxidation state from Mo^{6+} to Mo^{4+} is plausible due to two reasons. Firstly, ab initio calculations of Tossel (2005) showed that the reduction of Mo^{6+} (MoO_4^{2-}) to Mo^{5+} (MoO_4^{3-}) goes along with a fractionation towards light Mo isotopes. Secondly, MoO_4^{2-} species geometry is identical to that of SO_4^{2-}, which therefore may be taken as a first order analogue. Both anions show the relative heaviest isotope composition in low T processes. In addition, the SO_4^{2-} anion is also isotopically heavier when compared to other sulphur species with lower oxidation state (e.g. SO_2, FeS_2, $CuFeS_2$), at least up to 800 °C, (Ohomoto and Rye 1979). Therefore, the incorporation of light Mo^{4+} in molybdenite and common rock-forming minerals can account for the isotope fraction of processes Δ_1Mo and Δ_3Mo.

Molybdenum isotope fractionation between hydrothermal fluid and silicate melt, both assumed to be dominantly Mo^{6+} (O'Neill and Eggins, 2002; Zhang et al., 2012), requires another fractionation mechanism. It most likely relates to differences in Mo speciation between silicate melt and hydrothermal fluids. No agreement exists, however, on the predominant Mo complexes in hydrothermal fluids (see Rempel et al., 2009; Ulrich and Mavrogenes 2008; Zhang et al., 2012, and references therein). Our data clearly demonstrate that Mo isotope fractionation also occurs at the magmatic-hydrothermal transition, while the processes responsible for it remain to be determined.

6. Conclusions

The Mo isotope composition of molybdenite is used as a representative value for the Mo isotope signature of the continental input to the ocean (e.g., Arnold et al., 2004; Barling et al., 2001; Czaja et al., 2012; Dahl et al., 2011), an essential but highly debated value for mass balance models attempting to

reconstruct past ocean anoxia. Recent studies found a wide variability of δ^{98}Mo values of molybdenites (e.g., Hannah et al, 2007; Malinovsky et al., 2007; Mathur et al., 2010; Greber et al., 2011), which questions their applicability. Therefore we studied the δ^{98}Mo signature of molybdenites from the porphyry Questa Mo deposit (NM, USA), which is geochemically and petrologically well characterized. Our data demonstrate that Mo fractionated at three different occasions during the magmatic and hydrothermal history of the Questa deposit. All these Mo isotope fractionation processes lead to the enrichment of heavy Mo isotopes in the more evolved magma or fluid phase. Our results therefore imply that hydrothermal molybdenite Mo isotope data are positively biased from the source magma and thus from common evolved crustal rocks. It is likely that the first-order Mo isotope fractionation processes identified here are also applicable to other genetic types of molybdenite (e.g., skarn deposits); however, molybdenite occurrences related to granitic magmas are by far the most abundant. Therefore, we suggest that the Mo isotope mean value of molybdenites of ~0.4‰ (Greber et al., 2011) represents an upper limit of the average δ^{98}Mo of Earth's upper igneous crust.

Together with the study of Voegelin et al., (submitted), the data presented here built up a comprehensive framework explaining Mo isotope variability documented for igneous rocks and hydrothermal molybdenite. Based on these results and future investigations of crustal magmatic products, the crustal Mo isotope signature can be further refined.

Acknowledgments

Leonhard Klemm and Andreas Audétat are thanked for providing samples and sharing their knowledge about the Questa area. We are grateful to Dr. Christopher Pearce for constructive criticism and appreciate the editorial handling of Prof. Andrew Kerr. This work was supported by the Swiss National Science Foundation (SNSF Grants 200021–126759 to TFN and PP00P2-124370 to TP).

315

316 ## References

317 Archer, C., and Vance, D., 2008. The isotopic signature of the global riverine molybdenum flux and
318 anoxia in the ancient oceans. Nature Geoscience 1, 597–600.

319 Arnold, G.L., Anbar, A.D., Barling, J., and Lyons, T.W., 2004. Molybdenum Isotope Evidence for
320 Widespread Anoxia in Mid-Proterozoic Oceans. Science 304, 87-90.

321 Arnórsson, S., and Óskarsson, N., 2007. Molybdenum and tungsten in volcanic rocks and in surface and
322 <100°C ground waters in Iceland. Geochimica et Cosmochimica Acta 71, 284-304.

323 Audétat, A., and Pettke, T., 2003. The magmatic–hydrothermal evolution of two barren granites: a melt
324 and fluid inclusion study of the Rito del Medio and Canada Pinabete plutons in northern New
325 Mexico (USA). Geochimica et Cosmochimica Acta 67, 97–121.

326 Audétat, A., Pettke, T., Heinrich, C.A., and Bodnar, R.J., 2008. The composition of magmatic–
327 hydrothermal fluids in barren and mineralized intrusions. Economic Geology 103, 877-908.

328 Audétat, A., 2010. Source and Evolution of Molybdenum in the Porphyry Mo(–Nb) Deposit at Cave Peak,
329 Texas. Journal of Petrology 51, 1739-1760.

330 Audétat, A., Dolejš, D., and Lowenstern, J.B., 2011. Molybdenite Saturation in Silicic Magmas:
331 Occurrence and Petrological Implications. Journal of Petrology 52, 891-904.

332 Barling, J., Arnold, G.L., and Anbar, A.D., 2001. Natural mass-dependent variations in the isotopic
333 composition of molybdenum. Earth and Planetary Science Letters 193, 447-457.

334 Czaja, A.D., Johnson, C.M., Roden, E.E., Beard, B.L., Voegelin, A.R., Nägler, T.F., Beukes, N.J., and
335 Wille, M., 2012. Evidence for free oxygen in the Neoarchean ocean based on coupled iron–
336 molybdenum isotope fractionation. Geochimica et Cosmochimica Acta 86, 118-137.

337 Cline, J.S., and Bodnar, R.J., 1994. Direct evolution of brine from a crystallizing silicic melt at the Questa,

New Mexico, molybdenum deposit. Economic Geology 89, 1780–1802.

GERM, 2013, Geochemical Earth Reference Model – GERM: http://earthref.org/ (January 2013).

Greber, N.D., Hofmann, B.A., Voegelin, A.R., Villa, I.M. and Nägler, T.F., 2011. Mo isotope composition in Mo-rich high- and low-T hydrothermal systems from the Swiss Alps. Geochimica et Cosmochimica Acta 75, 6600-6609.

Greber, N.D., Siebert, C., Nägler, T.F. and Pettke, T., 2012. $\delta^{98/95}$Mo values and molybdenum concentration data for NIST SRM 610, 612, and 3134: towards a common protocol for reporting Mo data. Geostandards and Geoanalytical Research 36, 291–300.

Hannah, J.L., Stein, H.J., Wieser, M.E., de Laeter, J.R., and Varner, M.D., 2007. Molybdenum isotope variations in molybdenite: Vapor transport and Rayleigh fractionation of Mo. Geology 35, 703-706.

Holzheid, A., Borisov, A., and Palme, H., 1994. The effect of oxygen fugacity and temperature on solubilities of nickel, cobalt, and molybdenum in silicate melts. Geochimica et Cosmochimica Acta 58, 1975–1981.

Johnson, C.M, Lipman, P.W., and Czamanske, G.K., 1990. H, O, Sr, Nd, and Pb isotope geochemistry of the Latir volcanic field and cogenetic intrusions, New Mexico, and relations between evolution of a continental magmatic center and modifications of the lithosphere. Contributions to Mineralogy and Petrology 104, 99–124.

McKinlay, J.D., 1988. Compositionally zoned dikes of the Questa mine area, New Mexico: evidence for magma mixing and crystal fractionation, and implications for the evolution of the Questa magmatic system, Master thesis, University of Arizona.

Karlstrom, K.E., Whitmeyer, S.J., Dueker, K., Williams, M.L., Levander, A., Humphreys, G., Keller, G.R., and the CD-ROM Working Group, 2005. Synthesis of results from the CD-ROM

experiment: 4-D image of the lithosphere beneath the Rocky Mountains and implications for understanding the evolution of continental lithosphere, *in* Karlstrom, K.E. and Keller, G.R., eds, The Rocky Mountain Region -- An Evolving Lithosphere: Tectonics, Geochemistry, and Geophysics, American Geophysical Union Geophysical Monograph, 154, p. 421-441.

Klemm, L.M., Pettke, T., Heinrich, C.A., and Campos, E., 2007. Hydrothermal Evolution of the El Teniente Deposit, Chile: Porphyry Cu-Mo Ore Deposition from Low-Salinity Magmatic Fluids. Economic Geology 102, 1021-1045.

Klemm, L.M., Pettke, T., and Heinrich, C.A., 2008. Fluid and source magma evolution of the Questa porphyry Mo deposit, New Mexico, USA. Mineralium Deposita 43, 533-552.

Kuroda, P.K., and Sandell, E.B., 1954. Geochemistry of molybdenum. Geochimica et Cosmochimica Acta 6, 35–63.

Lipman, P.W., 1988. Evolution of silicic magma in the upper crust: The mid-Tertiary Latir volcanic field and its cogenetic granitic batholith, northern New Mexico, U.S.A. Transactions of the Royal Society of Edinburgh-Earth Sciences 79, 265–288.

Lipman, P.W., Mehnert, H.H., and Naeser, C.W., 1986. Evolution of the Latir volcanic field, Northern New Mexico, and its relation to the Rio Grande Rift, as indicated by potassium-argon and fission track dating. Journal of Geophysical Research 91, p. 6329–6345.

Malinovsky, D., Hammarlund, D., Ilyashuk, B., Martinsson, O., and Gelting, J., 2007. Variations in the isotopic composition of molybdenum in freshwater lake systems. Chemical Geology 236, 181-198.

Mathur, R., Brantley, S., Anbar, A., Munizaga, F., Maksaev, V., Newberry, R., Vervoort, J., and Hart, G., 2010. Variation of Mo isotopes from molybdenite in high-temperature hydrothermal ore deposits. Mineralium Deposita 45, 43-50.

Nägler, T.F., Anbar, A.D., Archer, C., Goldberg, T., Gordon, G.W., Greber, N.D., Siebert, C., Sohrin, Y.,

384 and Vance, D., 2013. Proposal for an International Molybdenum Isotope Measurement Standard
385 and Data Representation. Geostandards and Geoanalytical Research, doi: 10.1111/j.1751-
386 908X.2013.00275.x
387 Ohomoto, H., and Rye, R.O., 1979, Isotopes of Sulfur and Carbon, *in* Barnes H., ed., Geochemistry of
388 Hydrothermal Ore Deposits, John Wiley and Sons, New York.
389 O'Neill, H.S.C., and Eggins, S.M., 2002. The effect of melt composition on trace element partitioning: an
390 experimental investigation of the activity coefficients of FeO, NiO, CoO, MoO_2 and MoO_3 in
391 silicate melts. Chemical Geology 186, 151–181.
392 Pettke, T., Oberli, F., Audetat, A., Guillong, M., Simon, A., Hanley, J. and Klemm, L.M., 2012. Recent
393 developments in element concentration and isotope ratio analysis of individual fluid inclusions by
394 laser ablation single and multiple collector ICP–MS. Ore Geological Reviews 44, 10–38.
395 Pettke, Thomas. 2008. Analytical protocols for element concentration and isotope ratio measurements in
396 fluid inclusions by LA-(MC)-ICP-MS. Pages 189–218 of: Sylvester, P (ed), Laser ablation ICP-
397 MS in the Earth Sciences: Current practices and outstanding issues. Short Course Series, vol. 40.
398 Mineralogial Association of Canada.
399 Pietruszka, A., Walker, R., and Candela, P., 2006. Determination of mass-dependent molybdenum
400 isotopic variations by MC-ICP-MS: An evaluation of matrix effects. Chemical Geology 225, 121-
401 136.
402 Raimboult, L., and Burnol, L., 1998. The Richemont rhyolite dyke, Massif Central, France: A subvolcanic
403 equivalent of rare-metal granites. The Canadian Mineralogist 36, 265–282.
404 Rempel, K. U., Williams-Jones, A. E., and Migdisov, A. A., 2009. The partitioning of molybdenum(VI)
405 between aqueous liquid and vapour at temperatures up to 370°C. Geochimica et Cosmochimica
406 Acta 73, 3381-3392.

Rosera, J.M., Coleman, D.S., and Stein, H.J., 2013. Re-evaluating genetic models for porphyry Mo mineralization at Questa, New Mexico: Implications for ore deposition following silicic ignimbrite eruption. Geochemistry Geophysics Geosystems, doi: 10.1002/ggge.20048.

Ross, P.S., Jebrak, M.J., and Walker, B.M., 2002. Discharge of hydrothermal fluids from a magma chamber and concomitant formation of a stratified breccia zone at the Questa porphyry molybdenum deposit, New Mexico. Economic Geology 97,1679–1699

Siebert, C., Nägler, T.F., and Kramers, J.D., 2001. Determination of molybdenum isotope fractionation by double-spike multicollector inductively coupled plasma mass spectrometry. Geochemistry Geophysics Geosystems 2, art. no.-2000GC000124.

Siebert, C., Nägler, T.F., von Blanckenburg, F., and Kramers, J.D., 2003, Molybdenum isotope records as a potential new proxy for paleoceanography. Earth and Planetary Science Letters 211, 159-171.

Tossell, J.A., 2005. Calculating the partitioning of the isotopes of Mo between oxidic and sulfidic species in aqueous solution. Geochimica et Cosmochimica Acta 69, 2981-2993.

Ulrich, T., and Mavrogenes, J., 2008. An experimental study of the solubility of molybdenum in H_2O and KCl–H2O solutions from 500°C to 800°C, and 150 to 300MPa. Geochimica et Cosmochimica Acta 72, 2316-2330.

Voegelin, A.R., Pettke, T., von Niederhäusern, B., and Nägler, T.F., submitted. Magma differentiation fractionates Mo isotope ratios: Evidence from the Kos Plateau Tuff (Aegean Arc). Earth and Planetary Science Letters.

Wieser, M.E., and de Laeter, J.R., 2003. A preliminary study of isotope fractionation in molybdenites. International Journal of Mass Spectrometry 225, 177-183.

Wille, M., Kramers, J.D., Nägler, T.F., Beukes, N.J., Schroder, S., Meisel, T., Lacassie, J.P., and Voegelin, A.R., 2007. Evidence for a gradual rise of oxygen between 2.6 and 2.5 Ga from Mo

isotopes and Re-PGE signatures in shales. Geochimica et Cosmochimica Acta 71, 2417-2435.

Zajacz, Z., Halter, W. E., Pettke, T., and Guillong, M., 2008. Determination of fluid/melt partition coefficients by LA-ICPMS analysis of co-existing fluid and silicate melt inclusions: Controls on element partitioning. Geochimica et Cosmochimica Acta 72, 2169-2197.

Zimmerer, M.J., and McIntosh, W.C., 2012, The geochronology of volcanic and plutonic rocks at the Questa caldera: Constraints on the origin of caldera-related silicic magmas. Geological Society of America Bulletin 124, 1394–1408.

Zhang, L., Audétat, A., Dolejš, D., 2012. Solubility of molybdenite (MoS_2) in aqueous fluids at 600–800°C, 200MPa: A synthetic fluid inclusion study. Geochimica et Cosmochimica Acta 77, 175-185.

Table and figure captions

Figure 1. Simplified geological map of the area around the Questa porphyry Mo ore deposit after Ross et al. (2002) and Klemm et al. (2008). The small box on the left side illustrates the location of the Questa deposit. Sample locations are approximate. A detailed geological map can be downloaded for free at http://pubs.usgs.gov/imap/i-1907/.

Figure 2. A) Igneous magmatic-hydrothermal breccia sample with different clasts and a small, minor molybdenite-bearing vein. B) Stockwork vein sample. The vein cuts the surrounding rock and is highly enriched in molybdenite. A) and B) modified after Klemm et al., (2008).

Figure 3. Mo isotope data of molybdenites from the Questa porphyry Mo deposit, sorted according to their successive mineralization stage (x-axis; see text). Thick black bars are the median of the different magmatic-hydrothermal molybdenite crystallization stages. The grey bar sows the median δ^{98}Mo of the entire MHBX dataset. The black bar "Rhyolite, igneous leftover" at the bottom shows the Mo isotope composition of a syngenetic rhyolite, interpreted to represent the residual magma after fluid exsolution. A general trend towards heavier Mo isotope composition is visible with increasing fractionation of the system. Empty squares are the data of sample Nr.4 of unknown mineralization stage (Table 1). The black star shows the Mo isotope composition of the Bear Canyon granite. Overlapping values were slightly separated for clarity. δ^{98}Mo standard reproducibility is ≤ 0.1‰ (2SD). 2SE measurement uncertainty is typically around 0.05‰; data are listed in Table 1. MHBX = magmatic-hydrothermal breccia; STW= stockwork veins.

Figure S.1. Comparison between the element concentration of the Bear Canyon granite and the rhyolite sample. Major elements have very similar concentrations. The apparent enrichment of LREE in the Bear Canyon granite results from normalization to the Rhyolite sample which is very poor in LREE; absolute REE concentrations are low in both rocks. Note that none of the differences in element concentration between the Bear Canyon granite and the rhyolite is of similar magnitude as that documented for Mo (marked in red), which is 337 times stronger enriched in the Bear Canyon granite.

Table 1. δ^{98}Mo and Mo concentration data of molybdenites and igneous rocks from the Questa site.

Table S.1. Major and trace element composition of the rhyolite and Bear Canyon granite samples. Note the good agreement between the XRF, LA-ICP-MS and MC-ICP-MS (Table 1) concentration data.

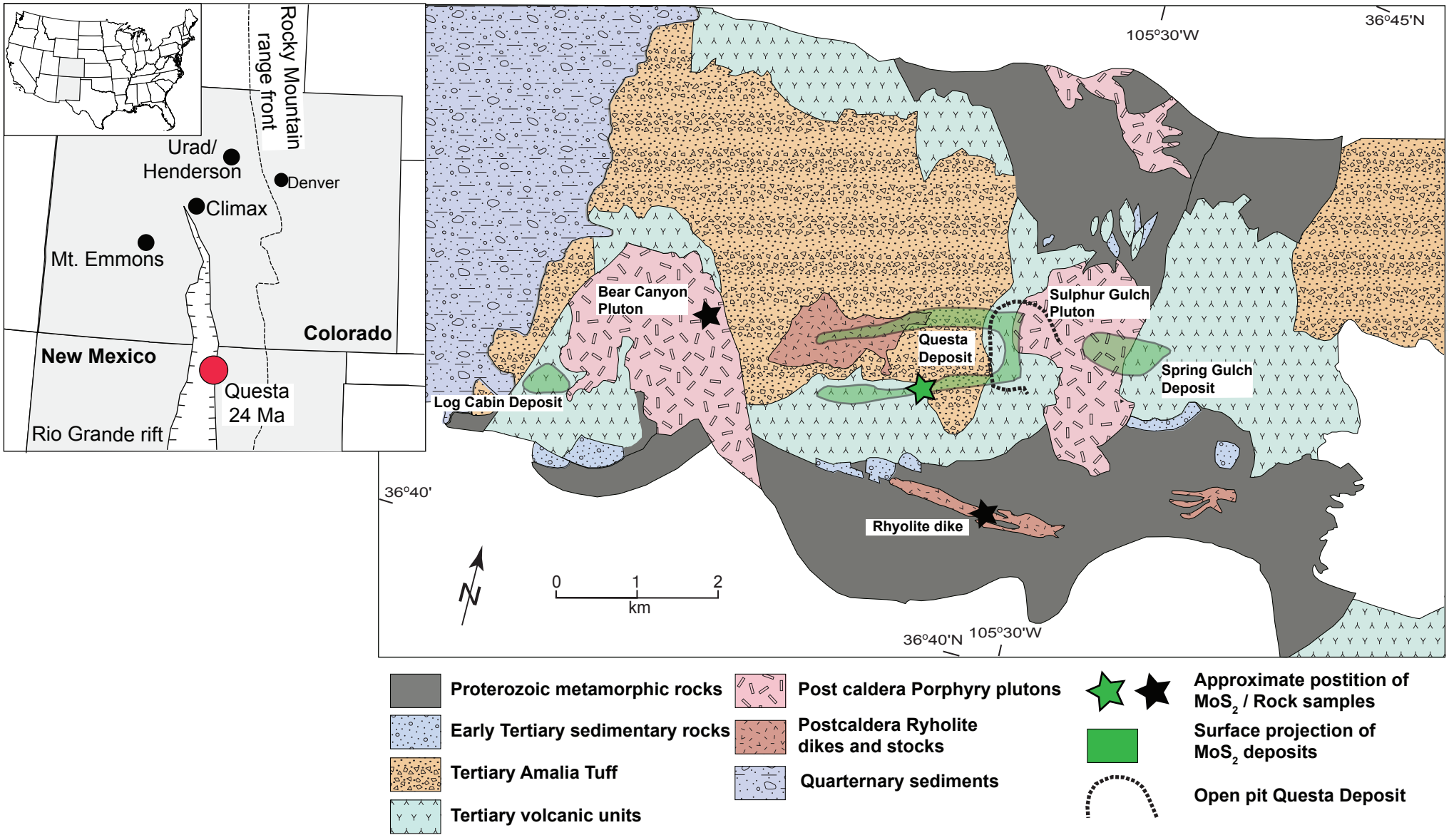
Rocky Mountain range front
Urad/ Henderson
Denver
Climax
Mt. Emmons
Colorado
New Mexico
Questa 24 Ma
Rio Grande rift
105°30'W
36°45'N
Bear Canyon Pluton
Sulphur Gulch Pluton
Questa Deposit
Spring Gulch Deposit
Log Cabin Deposit
Rhyolite dike
36°40'
0 1 2
km
36°40'N
105°30'W
Proterozoic metamorphic rocks
Early Tertiary sedimentary rocks
Tertiary Amalia Tuff
Tertiary volcanic units
Post caldera Porphyry plutons
Postcaldera Ryholite dikes and stocks
Quarternary sediments
Approximate postition of MoS2 / Rock samples
Surface projection of MoS2 deposits
Open pit Questa Deposit

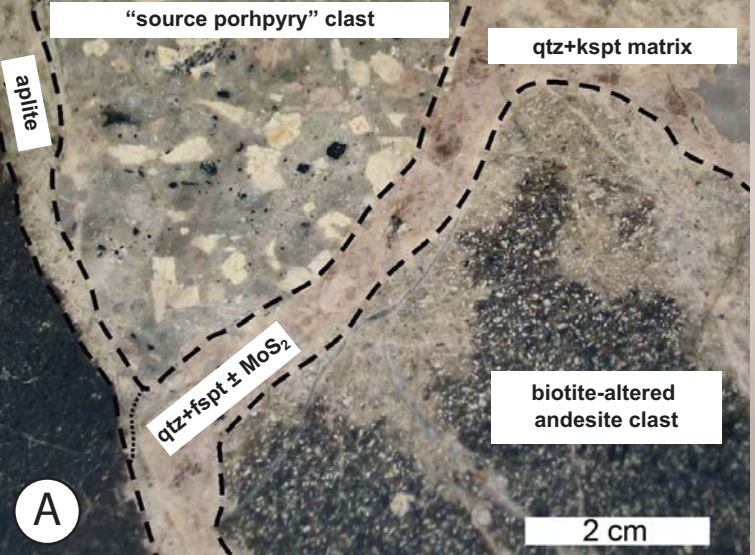
"source porhpyry" clast
qtz+kspt matrix
aplite
qtz+fspt ± MoS_2
biotite-altered
andesite clast
A
2 cm


B
2 cm

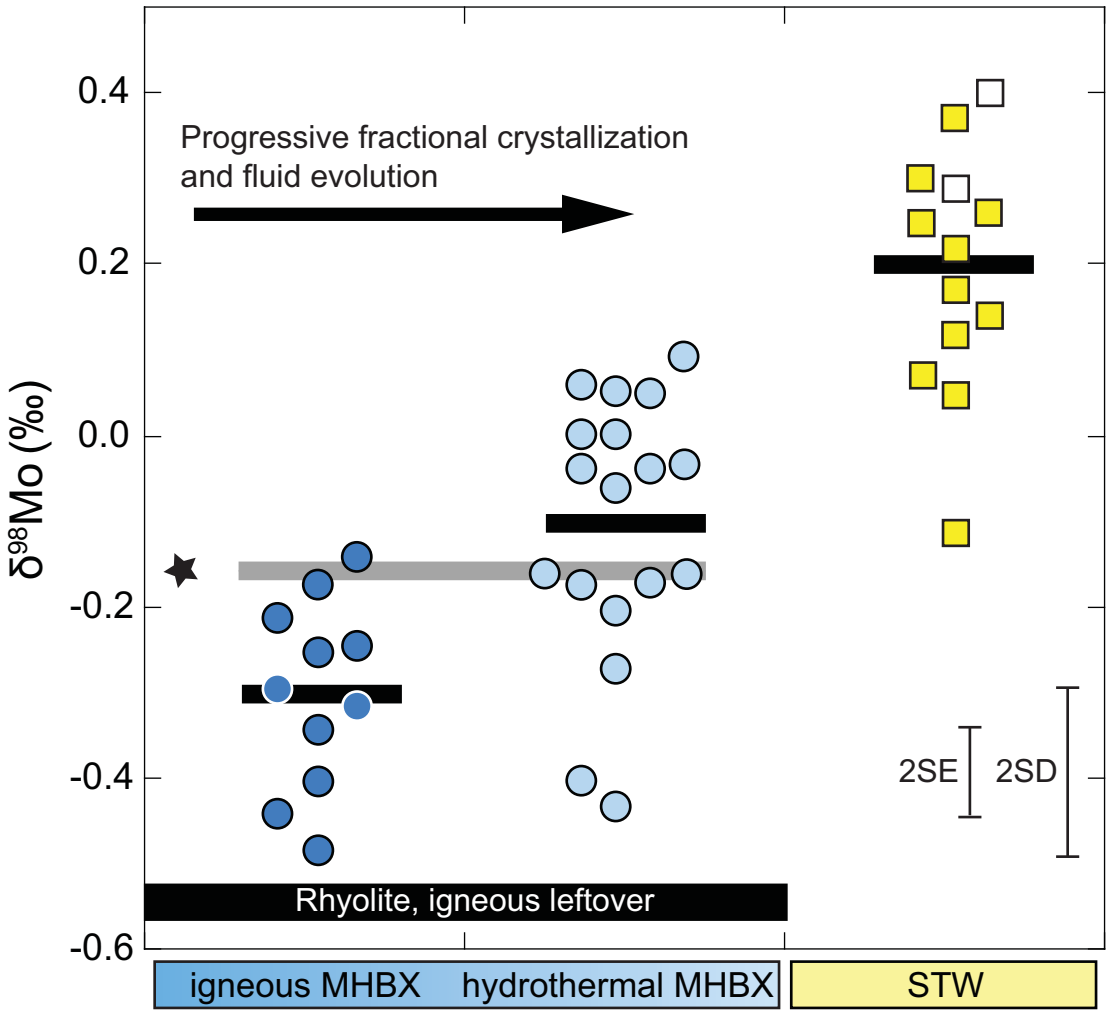
0.4
0.2
0.0
-0.2
-0.4
-0.6
δ98Mo (‰)
Progressive fractional crystallization
and fluid evolution
2SE
2SD
Rhyolite, igneous leftover
igneous MHBX
hydrothermal MHBX
STW

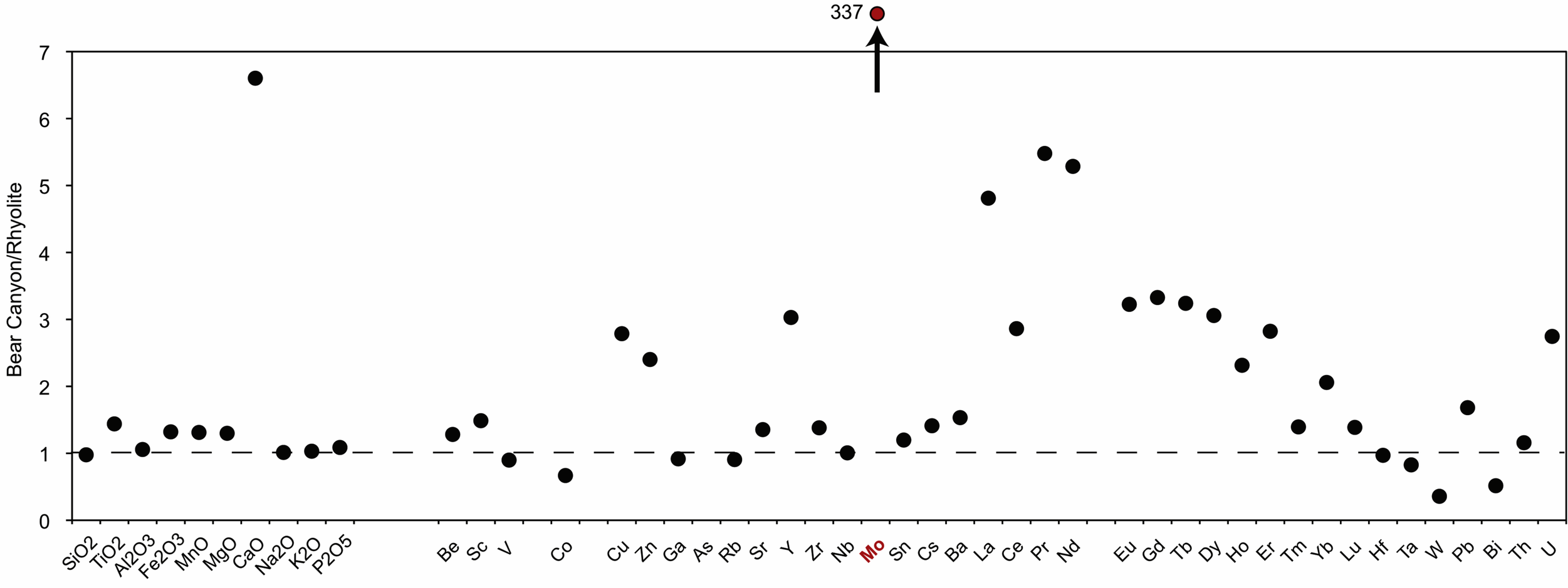
337
Bear Canyon/Rhyolite
0
1
2
3
4
5
6
7
SiO2
TiO2
Al2O3
Fe2O3
MnO
MgO
CaO
Na2O
K2O
P2O5
Be
Sc
V
Co
Cu
Zn
Ga
As
Rb
Sr
Y
Zr
Nb
Mo
Sn
Cs
Ba
La
Ce
Pr
Nd
Eu
Gd
Tb
Dy
Ho
Er
Tm
Yb
Lu
Hf
Ta
W
Pb
Bi
Th
U

Table 1. δ^{98}Mo and Mo concentration data of molybdenites and igneous rocks from the Questa site.

Stage/Name	Sample		[Mo] (µg g^{-1})	δ^{98}Mo (‰)	2SE	Mean value	Median	Minimum	Maximum
Molybdenites									
igneous MHBX	QDU 2 2	a	nd	-0 14	0 04				
		b	nd	-0 21	0 03				
		c	nd	-0 48	0 03				
		d	nd	-0 17	0 04				
		e	nd	-0 24	0 05				
		f	nd	-0 34	0 04				
	QDU 2	a	nd	-0 25	0 04				
		b	nd	-0 29	0 04				
		c	nd	-0 40	0 05				
	QDU A	a	nd	-0 44	0 08				
		b	nd	-0 31	0 05	-0 30	-0 29	-0 48	-0 14
hydrothermal MHBX	QDS 2	a	nd	-0 17	0 05				
		b	nd	0 05	0 05				
		c	nd	-0 16	0 05				
	QDS 2 2	a	nd	-0 16	0 04				
		b	nd	-0 17	0 04				
		c	nd	-0 03	0 05				
	QDS 4 3	a	nd	0 00	0 05				
		b	nd	-0 06	0 03				
		c	nd	0 00	0 04				
		d	nd	-0 04	0 07				
	QDS 4 4	a	nd	0 05	0 05				
		b	nd	0 09	0 05				
		c	nd	0 06	0 05				
		d	nd	-0 04	0 04				
	QDS 4 8	a	nd	-0 20	0 05				
		b	nd	-0 43	0 04				
		c	nd	-0 27	0 04				
		d	nd	-0 40	0 03	-0 10	-0 05	-0 43	0 09
Stockwork	QDS 3	a	nd	0 37	0 05				
		b	nd	0 26	0 04				
		c	nd	0 22	0 06				
	QDS 3 1	a	nd	0 07	0 04				
		b	nd	0 12	0 07				
		c	nd	0 14	0 04				
		d	nd	0 25	0 05				
	QDS 3 2	a	nd	0 05	0 05				
		b	nd	0 30	0 05				
		c	nd	-0 11	0 03				
		d	nd	0 17	0 03				
	Nr 4*	a	nd	0 29	0 06				
		b	nd	0 40	0 05	0 20	0 22	-0 11	0 40
Rocks									
Granite, Bear Canyon Pluton†		a	39 1	-0 13	0 03				
		b	41 9	-0 18	0 03	-0 16	-	-	-
Rhyolite dike		a	0 12	-0 56	0 06				
		b	0 12	-0 58	0 05	-0 57	-	-	-

*Unknown mineralization stage, but interpreted to belong to the Stockwork (see text)

†Due to its [Mo] and δ^{98}Mo interpreted to be influenced by a molybdenite mineralization event (Log Cabin, see discussion)

All Mo isotope data is relative the JMC ICP solution lot 602332B δ^{98}Mo standard reproducibility is ≤ 0 1‰

NIST SRM 3134 Mo standard = 0 25‰ (see Greber et al , 2012)

2SE is the within run error of an individual measurement

nd = not determined

Supplementary Table. Major and trace element composition of the rhyolite and Bear Canyon granite samples.

Element	Isotope analyzed LA-ICP-MS		Rhyolit XRF	Rhyolit LA-ICP-MS	1 SD	Bear Canyon granite XRF	Bear Canyon granite LA-ICP-MS	1 SD	Bear Canyon/Rhyolit
SiO2		wt.%	77.95	-		76.22	-		0.98
TiO2	49	wt.%	0.09	0.096	0.001	0.14	0.138	0.004	1.44
Al2O3		wt.%	12.10	-		12.79	-		1.06
Fe2O3		wt.%	0.73	-		0.96	-		1.32
MnO	55	wt.%	0.03	0.029	0.001	0.04	0.038	0.001	1.31
MgO		wt.%	0.14	-		0.18	-		1.30
CaO		wt.%	0.10	-		0.64	-		6.60
Na2O		wt.%	3.95	-		4.00	-		1.01
K2O		wt.%	4.43	-		4.56	-		1.03
P2O5	31	wt.%	0.02	0.032	0.002	0.03	0.035	0.002	1.09
LOI		wt.%	0.57	-		0.50	-		
Total			100.1			100.1			
Be	9	µg g^{-1}	-	5.85	1.23	-	7.50	1.78	1.28
Sc		µg g^{-1}	3.9	nd		5.8	nd		1.49
V		µg g^{-1}	7.9	nd		7.1	nd		0.90
Cr		µg g^{-1}	3.6	nd		<2.8	nd		-
Co	59	µg g^{-1}	<2.6	1.35	0.14	<2.6	0.90	0.15	0.67
Ni	62	µg g^{-1}	4.3	<5 1		<4.1	<6.6	-	-
Cu	65	µg g^{-1}	6.3	2 11	0.23	7.9	5.88	0.38	2.79
Zn	66	µg g^{-1}	17.8	15.1	2.0	42.0	36.2	2.6	2.40
Ga	71	µg g^{-1}	23.8	18.7	1.9	24.9	17.2	1.0	0.92
As	75	µg g^{-1}	-	<1.7		-	<1.4	-	-
Rb	85	µg g^{-1}	173.6	189.0	10.7	167.2	171.3	1 5	0.91
Sr	88	µg g^{-1}	56.9	58.1	2.0	82.6	78.7	1.8	1.35
Y	89	µg g^{-1}	<1.1	2.48	0.18	7.0	7.51	0.28	3.03
Zr	90	µg g^{-1}	67.9	72.9	3.6	105.3	100.7	2.7	1.38
Nb	93	µg g^{-1}	24.9	27.0	0.9	25.8	27.2	0.7	1.01
Mo	95	µg g^{-1}	-	<0.48		-	40.72	2.56	337
Sn	118	µg g^{-1}	-	2.26	0.46	-	2.70	0.39	1.20
Cs	133	µg g^{-1}	-	0.92	0.07	-	1.30	0.06	1.41
Ba	137	µg g^{-1}	174.1	206	2	295.4	316	6	1.53
La	139	µg g^{-1}	10.2	5.77	0.28	23.3	27.76	0.37	4.81
Ce	140	µg g^{-1}	-	16.0	0.1	-	45.8	1.6	2.86
Pr	140	µg g^{-1}	-	0.71	0.03	-	3.87	0.32	5.48
Nd	146	µg g^{-1}	-	1.99	0.18	-	10.51	0.98	5.29
Sm	147	µg g^{-1}	-	<0.42		-	1.31	0.15	-
Eu	151	µg g^{-1}	-	0.083	0.022	-	0.27	0.07	3.22
Gd	157	µg g^{-1}	-	0.29	0.16	-	0.97	0.14	3.33
Tb	159	µg g^{-1}	-	0.045	0.028	-	0.15	0.03	3.24
Dy	163	µg g^{-1}	-	0.33	0.07	-	1.00	0.15	3.06
Ho	165	µg g^{-1}	-	0.085	0.001	-	0.20	0.03	2.32
Er	167	µg g^{-1}	-	0.30	0.09	-	0.85	0.10	2.82
Tm	169	µg g^{-1}	-	0.083	0.022	-	0.12	0.02	1.39
Yb	173	µg g^{-1}	-	0.61	0.09	-	1.25	0.42	2.06
Lu	175	µg g^{-1}	-	0.17	0.03	-	0.24	0.06	1.39
Hf	178	µg g^{-1}	-	3.61	0.34	-	3.51	0.12	0.97
Ta	181	µg g^{-1}	-	2.33	0.17	-	1.93	0.09	0.83
W	182	µg g^{-1}	-	2.91	0.20	-	1.04	0.07	0.36
Pb	208	µg g^{-1}	-	12.6	1.8	-	21.2	0 9	1.68
Bi	209	µg g^{-1}	-	0.50	0.18	-	0.26	0.03	0.52
Th	232	µg g^{-1}	24.6	23.8	1.2	28.6	27.6	0 9	1.16
U	238	µg g^{-1}	5.0	4.49	0.32	12.2	12.3	0 5	2.75

Bear Canyon/Rhyolite; if available always LA-ICP-MS data used, otherwise XRF or MC-ICP-MS
nd = not determined due to polyatomic Li-B-Ar interferences
<x.x = below limit of detection, calculated for the LA-ICP-MS data following Pettke et al., 2012